

MEMS-based OBN: lessons learnt from the largest OBN survey worldwide

Nicolas Tellier^{1*} and Philippe Herrmann¹ demonstrate the value of micro-electromechanical systems-based digital seismic accelerometers for ocean bottom node seismic projects.

Abstract

Despite a recovery in the number of towed-streamer surveys being conducted, OBN (Ocean Bottom Node) seismic projects continue to take an increasing market share over towed-streamer surveys. In OBN acquisition, each node is equipped with a pressure sensor (hydrophone) and three motion sensors (typically, geophones). The nearly-a-century-old geophone technology has, however, certain inherent shortcomings that degrade the recorded signal. Geophone performance deviates from reference specifications due to manufacturing tolerances, ageing and changes in temperature. As an example, for 15-Hz omnitilt geophones, as commonly used in OBN acquisitions, the variation in response reaches 3 dB in amplitude and 10 degrees in phase within their range of manufacturing tolerances. These uncertainties in sensor response prove particularly difficult to model and correct for in practice and result in final data sensor artefacts. The insensitivity of geophones to the gravity field also requires the use of additional tilt meters for the verticalisation of the 3C with resulting issues related to the relative orientations of these two pieces of equipment.

Today, MEMS (Micro-Electromechanical Systems)-based digital seismic accelerometers have proved to be the high-fidelity alternative to geophones. Their specifications are not affected by temperature, ageing or manufacturing tolerances, making the recorded signal accurate in phase and amplitude with the seismic signal over the entire seismic bandwidth. As MEMS can detect the gravity vector, the integration of this sensing technology into OBN has demonstrated that 3C MEMS provide, without pre-processing, seismic signal with true verticality, and a vector fidelity error (error in orthogonality between the three sensors) that is an order of magnitude lower than for 3C geophones. The excellent low-frequency performance of the latest, third-generation MEMS is also ideal for reaping the full benefit of novel low-frequency sources (Ronen 2017), and in this way pushing back further the limits of FWI.

This, along with other MEMS properties, makes this sensor a strong driver for the growth of OBN acquisition – especially for sparse or blended acquisition, where sensor fidelity matters more than ever. At the time of writing, the world's largest OBN survey is continuing in the Middle East and is starting to deliver a promising dataset from the 23,000 MEMS-based OBNs

deployed. Observations from this mega-survey, as well as from a previous experimental survey that includes direct comparisons with geophone-based OBN, are presented and discussed in this article.

Introduction — A MEMS update

MEMS sensors are becoming increasingly common in our daily lives. This may actually be an understatement, as they are in fact everywhere around us. As an example, they equip vehicles, triggering airbags when a sharp deceleration is detected. They detect user movements on consumer electronics, such as smartphones, game controllers or augmented reality devices, enabling advanced interactions with these devices. MEMS are also now found in printers, microscopes, barometers and LIDAR, as well as in numerous other industrial applications.

MEMS stands for Micro Electro-Mechanical Systems. Made of silicon, they incorporate both electronic and mechanical moving parts. While they were initially used to measure mainly motion (through acceleration), they have steadily proven their value to sense many other physical quantities, such as temperature, pressure, stress and strain. Their microscopic scale is a big advantage for sensing: they are gradually replacing conventional transducers, to a point where sensing insiders refer to the 'second silicon revolution' (the first one being silicon electronic chips, the second mechanical structures used to sense any physical property), and how the existing sensing market is being disrupted.

However, even today, there are not that many MEMS acceleration sensors available for seismic applications. Their technical specifications must be carefully defined to sense the seismic wavefield of interest. This wavefield must be equally sensed within the entire seismic bandwidth of interest over its 120 dB + dynamic range, from the smallest signal (weak and deep reflections recorded at long offsets) to the strongest (near offsets with impulsive sources). For seismic applications, MEMS sensors must also be robust, and sufficiently reliable to survive the rigours of deployment on operational seismic crews. But designing a properly specified MEMS is not enough. MEMS are fully integrated with their related electronics on acquisition unit PCBs (Printed Circuit Boards) that control the MEMS and manage their outputs. In a microscopic context, the physical quantities at stake, managed by the electronics, are also orders

¹ Sercel

* Corresponding author, E-mail: nicolas.tellier@sercel.com

DOI: 10.3997/1365-2397.fb2023093

of magnitudes below those of conventional sensors. The quality of the electronics is therefore paramount: the signal recorded by the best MEMS would be compromised if integrated into poorly specified electronics. Developing a MEMS sensing solution with the associated low-consumption electronics requires years of development and significant investment.

In terms of performance, MEMS enjoy several advantages when compared to the alternative sensing technologies commonly used in seismic acquisition. They are immune to electro-magnetic noise, are not affected by spurious frequencies, and exhibit low distortion. Made of pure silicon, they do not age like geophones or piezoelectric sensors. More importantly, the third generation of MEMS sensors (Lainé 2014) meets industry requirements for high-fidelity low frequencies, which they record with true amplitude and phase (i.e., they are not subject to ‘data jitter’ (Tellier, 2021)). In OBN acquisition, MEMS are used in 3C for vectorial applications such as node reorientation and shear wave sensing. When combined with a hydrophone, 3C MEMS also perform wavefield separation according to the wave direction of propagation. They already enjoy a proven track record of success in ocean-bottom cable systems (e.g., SeaRay system, Archer 2012, Keggins 2017). As MEMS sense acceleration with a constant sensitivity whatever the frequency and without any phase delay, they are perfect zero-phase broadband sensors.

The first OBN system equipped with 3C MEMS sensors has been introduced recently. The GPR300 embeds 3C QuietSeis™ MEMS purpose-built for seismic acquisition, with a so far unequalled performance in the industry. Seismic data from two acquisitions – an experimental deployment alongside geophone-based OBN, and a commercial survey with MEMS-based OBN operated in stand-alone mode – have been analysed in depth. The results demonstrate obvious benefits for state-of-the-art MEMS sensors when deployed in an OBN setting.

Experimental acquisition

The value of 3C MEMS for OBN acquisition was assessed on a commercial survey, where standard ocean-bottom nodes integrating 3C omni-tilt 15 Hz geophones were being used. For this experiment in a shallow depth context (20-30 m), a line of 28 MEMS-based OBNs was also deployed with the commercial spread. The two types of nodes were collocated (distance < 1 m),

and each receiver station spaced 100 m apart. A 10 km source line was shot with a 25 m source interval (Figure 1).

Only basic processing was applied for the sensor CRGs (Common Receiver Gathers) shown in figures 2, 3 and 4, for the purpose of obtaining genuine sensor comparisons, without hypothesis or biases introduced by processing geophysicists. Sensor de-signature from mV to m.s⁻¹ was performed (for geophones: phase and amplitude compensation for natural frequency, damping and sensitivity; for MEMS: integration from acceleration to velocity and sensitivity compensation). The vertical component (Z) was reconstructed by using the tilt sensor measurement for geophones and the built-in sensor tilt determination for MEMS.

Outcome #1: true verticality

State-of-the-art, high-fidelity MEMS accelerometers are fitted with a feedback loop that enables the measurement of static (0 Hz) signals, such as Earth’s gravity. Each of the three MEMS therefore detects its own tilt error: the actual tilt of the OBN can then be computed with a high degree of fidelity from these three values, and the Z component perfectly projected on the vertical. This can be compared favourably to embedded ancillary tilt sensors used in geophone OBNs, specified with a +/- 1.5° typical tilt precision (not accounting for the uncertainty in angle between the tiltmeter and the 3C phones), and requiring a mandatory pre-processing step to verticalise the seismic data.

The CRGs presented in figure 2 compare the Z components from the two OBN families. With the application of a 1500 m/s linear moveout (LMO) to correct for water velocity, the water break would get flattened at t=0. As the experimental acquisition was performed in shallow water and acquired with long offsets, recording the water break is not expected on the reconstructed Z component. While it is the case for the Z MEMS, the water break is still apparent on the Z geophone data. Observations are similar for the guided waves, polarised quasi-horizontally: they are almost absent from the Z MEMS record, but prevalent on the Z geophone record. The quality of the vertical reorientation enabled by a direct measurement (tiltmeter for geophones, and direct sensing of the gravity for MEMS) is therefore paramount. Indeed, a vertical reorientation of the geophone Z data at the processing stage, on the basis of seismic data, proves quite difficult due to strong interference between waves in a shallow water context.

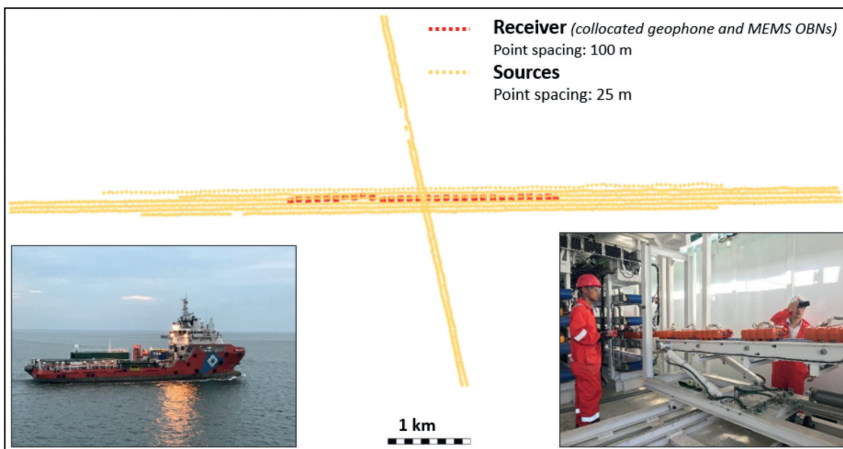


Figure 1 Experimental acquisition: acquisition diagram, (bottom left) node vessel, (bottom right) back deck node deployment. Courtesy of BGP.

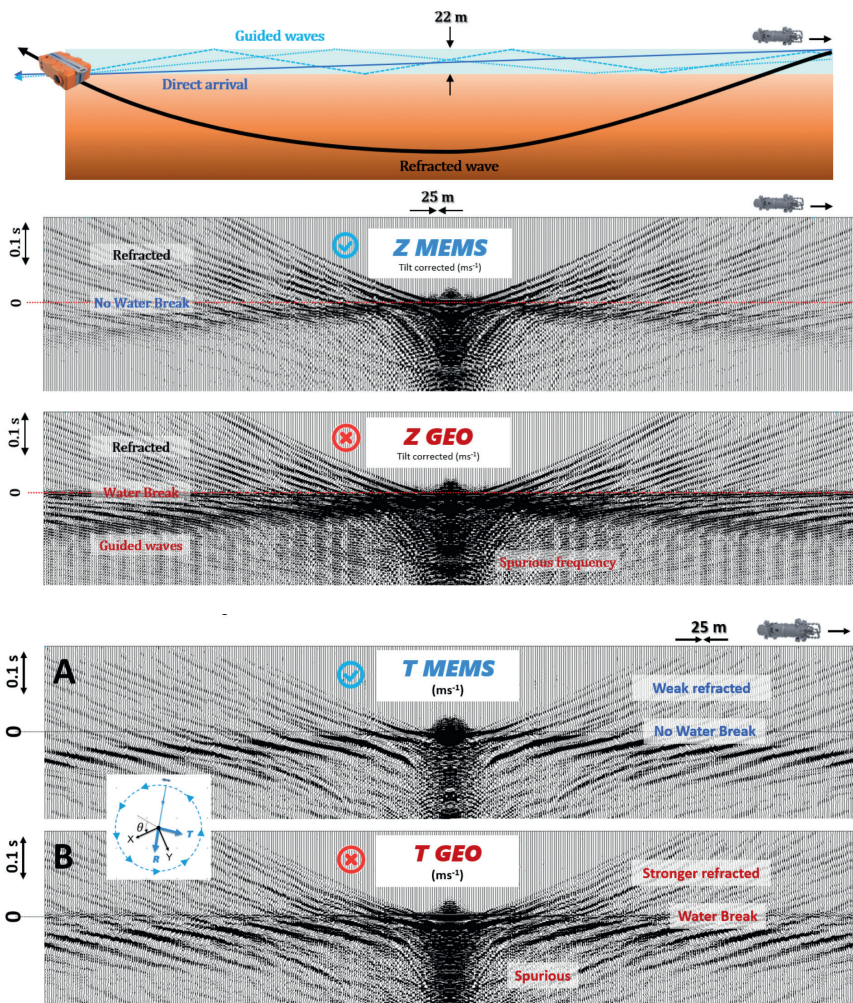


Figure 2 (Top) In a shallow-water (22 m depth difference between sources and receivers) and long-offset setting, seismic signal polarised quasi-horizontally (such as the direct arrival and guided waves) is not expected on the Z component. CRGs, after application of a 1500 m/s LMO, confirm an excellent verticality for the MEMS (middle), but not for the geophones (bottom).

Figure 3 CRGs after application of a 1500 m/s LMO and projected in the transverse direction of the source-node referential.

This would be the same for a blended acquisition, which is a standard now for OBN operations.

3C MEMS therefore enable the delivery of seismic data polarised vertically with no verticality error and no pre-processing. In addition, as the tilt value is continuously monitored and inscribed in the header, continuous monitoring of the node orientation becomes possible (described in more detail in outcome #6).

Note that a sensor artefact can be observed on the Z geophones, with the observation of spurious noise. Spurious noise is caused by the lateral resonance of the geophone mass-spring system and occurs in the high frequencies (> 150 Hz, depending on the geophone model used). Though outside the seismic bandwidth of interest for this given acquisition, all 28 geophone-based OBNs did display such spurious noise.

Outcome #2: 3C vector fidelity

Good MEMS accelerometers can measure static signals such as the Earth's gravity. Thanks to this feature, 3C MEMS sensors can easily be factory-calibrated for orthogonality. After gravity-driven calibration, the three MEMS are almost perfectly orthonormal (0.25° in the worst case). This is not the case with 3C geophones: their orthogonality relies only on the manufacturing precision of the 3C assembly hosting the sensors. For any mechanical manufacturing process, precision is a matter of price. While a 1-degree error between orthogonal axes is easily achievable in

3C geophone manufacturing, attempting to achieve zero degree error makes the manufacturing cost exponential. In addition to this residual error, the alignment error of the geophones in their casings has to be considered. This limitation combined with an inherent 'data jitter' makes 3C geophones only approximately orthonormal, with no means to correct for it at a later stage.

Similarly, and contrary to the case with 3C geophones, the particle motion measured in the field by 3C MEMS can be projected along an exact vertical (Z) axis which, owing to the 3C orthonormality, ensures two perfectly horizontal (X,Y) axes for the entire duration of the recording time, from node deployment to node recovery. As a result, 3C MEMS sensors with 0 Hz capability demonstrate an excellent vector fidelity, which, combined with their true-amplitude capability and excellent cross-axis rejection, enable thorough separation of the polarisation of the different wave types and rigorous polarisation analysis. The high-fidelity data recorded in this way avoids the need for data-driven sensor rotation solutions with projections onto the vertical axis that have numerous limitations relating to processing software, operator practices, water depth, offset and azimuthal coverage, data signal-to-noise ratio and bandwidth, as well as on the level of contamination between interfering blended sources.

Figure 3 displays horizontal CRGs after LMO correction to account for water velocity, projected onto the signal radial and transverse directions. Rotation from the node (X,Y) reference to the

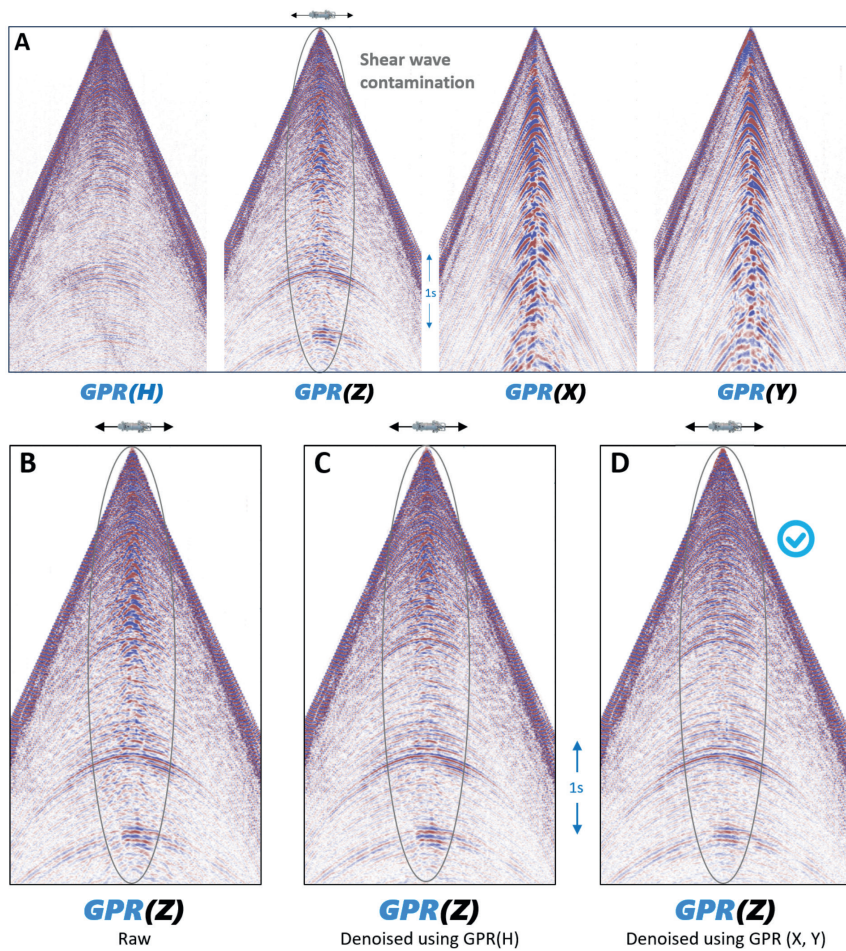


Figure 4 Z MEMS shear wave denoising: A) Display of the four recorded components (from left to right: hydrophone, Z, X and Y MEMS). B) Raw Z CRGs (repeated from A) display strong shear wave contamination at short offsets. C) The common approach to addressing this noise is based on Z component calibration with the hydrophone. D) A 3C sensor system showing excellent vector fidelity contains the entire wavefield, without any information loss. The X and Y components therefore enable almost perfect denoising.

source-node (radial/transverse) reference was performed after a scan of azimuths, on the basis of the θ angle that minimises at best the transverse/radial energy ratio. For the source-node reference, the quality of vector fidelity can be assessed from the residual energy present on the transverse direction. The overall energy of the MEMS transverse data (Figure 3a) proves to be significantly lower than its geophone counterpart (Figure 3b). On these CRGs, the water break is also slightly apparent and the refracted waves stronger on the geophone data, confirming the superior vector fidelity of MEMS. The better reorientation achieved with 3C MEMS proves beneficial for seismic-driven node azimuthal reorientation.

Outcome #3: value of horizontal components

The value of horizontal data in OBN acquisition is three-fold. Their primary value lies in all applications that make use of the timing and polarisation of the water break, such as the reorientation, from the node reference to the acquisition one. Indeed, and in contrast to hydrophones, motion sensors are directional, and optimised to sense seismic signal from one direction only. Integrating motion sensors with an excellent cross-axis rejection has been essential in the development of this ocean-bottom node, by combining the QuietSeis MEMS with gravity-assisted orthonormalisation. The second value lies in PS imaging. Though not a standard, owing to its intrinsic complexity, PS imaging is highly valued, for example in South-East Asia, to solve PP signal attenuation created by the presence of numerous gas clouds.

Analysis of the data recorded enabled the identification of a third benefit: the advanced denoising capability enabled by 3C MEMS. With an excellent vector fidelity and a superior cross-axis rejection, the full wavefield is recorded and signal polarisation is preserved. Figure 4a shows CRGs of the four components of the MEMS-based OBN. Figure 4b displays a raw CRG record that is highly contaminated by shear signal at short offsets. Removing this contamination is a standard processing step, based on calibration of the Z motion data with the hydrophone data. Figure 4c demonstrates the efficiency of this approach, but also its limitations as some PS contamination is still observed at short offsets. When using the full wavefield recorded by 3C MEMS instead of the hydrophone (Figure 4d), the denoising process leaves almost no residual contamination in the Z CRG and delivers to processing geophysicists the clean short offsets expected to compute calibration operators for deghosting purposes.

Outcome #4: sensor complementarity

The excellent complementarity of the hydrophone with MEMS motion sensors was further demonstrated when a basic notch in-fill of the hydrophone data was performed with the Z MEMS one (Figure 5). Here again, the processing remained elementary and deterministic, with no processing assumptions or parametrisation. Starting from native hydrophone data and time-integrated Z MEMS data on the one hand and native hydrophone data and Z geophone data not corrected for its natural frequency on the other, we computed Z scalars to illustrate how Z amplitude spectra com-

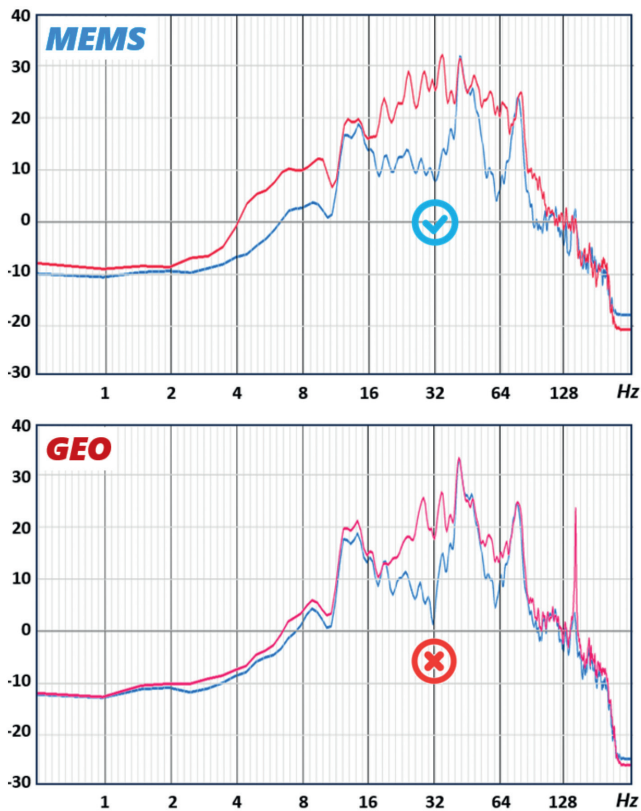


Figure 5 Field data spectra: (blue) hydrophone data, (red) hydrophone data after a basic notch filling process.

plementary to the hydrophone amplitude spectra. The notch in-fill is significantly improved, an outcome supported by the superior fidelity and consistency of the MEMS at these frequencies. As for the CRG shown in figure 2, the spurious frequency of the geophones can be observed, around 150 Hz.

Commercial acquisition

A mega-survey has been underway in Abu Dhabi since October 2021. It is part of the largest continuous 3D survey ever performed (Cambois, 2019) and covers both onshore and offshore objectives. This acquisition is taking place in shallow waters from 0 to 25 m water depths and is deploying 23,000 MEMS-based OBNs (Figure 6), the largest node inventory ever used for seabed acquisition. A portion of the OBNs are also being deployed on the foreshore, which is regularly covered and uncovered by tides. Unlike the experimental acquisition presented above, this commercial survey did not involve the use of geophones which makes further direct comparison impossible. However, several

additional observations could be made on the geophysical value of the 3C MEMS, and on the accuracy of the synchronisation approach performed on the node in which the sensors are embedded.

Outcome #5: low frequencies

One of the key requirements for this survey is the quality of the low-frequency signal acquired. Although dedicated low-frequency sources (e.g., Shang, 2023) were not employed for the acquisition, the design of the airgun array yielded adequate low-frequency performance and makes it possible to assess the performance of the two types of sensors embedded in the node – MEMS and hydrophones.

MEMS sensors have evolved. The first generations were not optimised for low frequencies, as, at the time of their release, before 2010, the industry was not largely concerned with such frequencies. The third generation of MEMS (QuietSeis™) was developed and released for the specific purpose of meeting today's industry expectations for low frequencies and after years of research and development required to meet the industry standard. At low frequencies and at a microscopic scale, all types of noise need to be properly identified and addressed. Validating sensor performance also requires purpose-built test facilities, such as a low-noise underground laboratory (Lainé 2014).

MEMS sensors have a particular advantage over moving coil geophones. As they are effectively not affected by manufacturing tolerances, ageing and temperature variations, their response is exact in phase and practically true in amplitude. Deconvolving for the sensor response ('de-signature') requires the application of a pseudo-sensitivity value, which is a fixed scalar (further information on sensor technologies is provided e.g. in Tellier, 2017). As a result, the conversion from measurement units (24-bit digital) to physical quantities (acceleration, $m.s^{-2}$) is exact (Figure 7, right), as is the integration into other physical domains of interest (velocity, $m.s^{-1}$), and ever more frequently displacement (m) (Cordery, 2020). The consistency and fidelity of the signal acquired with MEMS sensors therefore favours their use for time-lapse (4D) or monitoring purposes.

This is not the case with geophones. Performing a robust designation process requires prior knowledge of several parameters (damping, natural frequency and sensitivity) that define the sensor response. In practice, these parameters are affected by significant variations in manufacturing tolerances, while also being susceptible to ageing (with the magnet losing its magnetic properties) and temperature variations. Retrieving the specific values of each individual geophone is impractical in the field

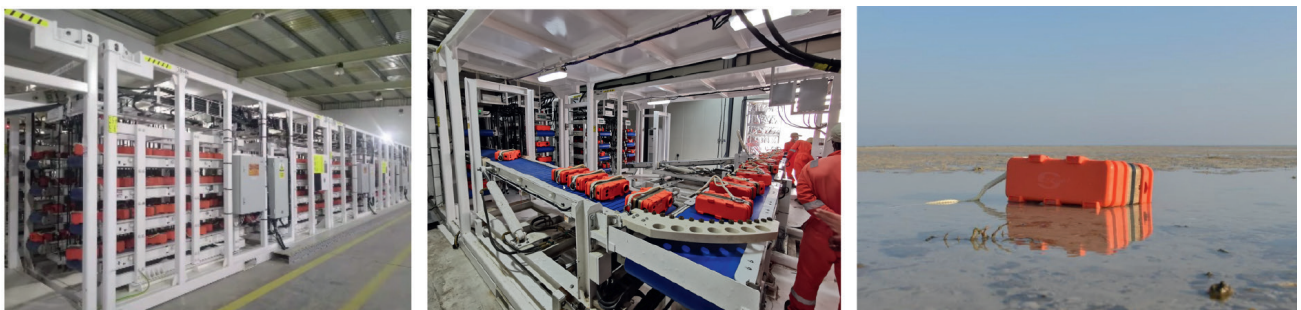


Figure 6 Field context: (left and centre) GPR300 on LARS (launch and recovery system) ready for deployment, (right), A node laid out and anchored on the foreshore.

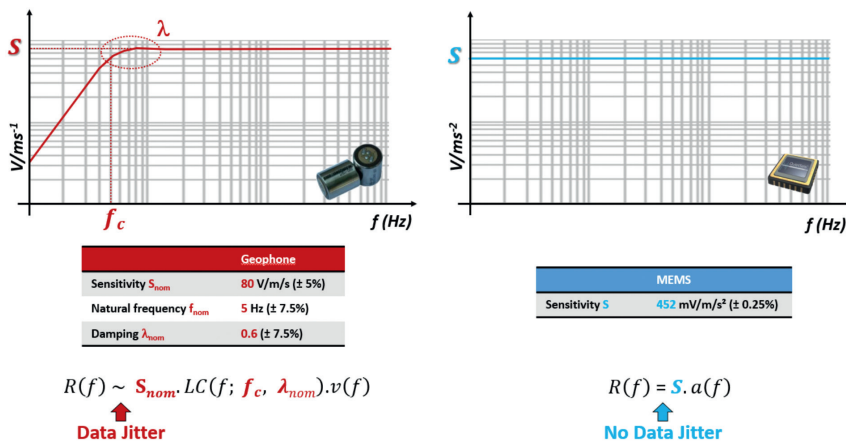


Figure 7 Designature approach with the inherent responses of geophones (left, illustrated for a 5 Hz geophone) and MEMS (right). $R(f)$ refers to raw sensor responses, $\theta(f)$ and $a(f)$ to the ground particle velocity and acceleration, respectively. For geophones, $LC()$ refers to a 2nd order designature operator. The absence of actual values for individual geophones (with account of tolerances) does not allow for an exact retrieval of the ground particle velocity from the raw responses deconvolved using nominal parameters ($S_{nom}, f_{nom}, \lambda_{nom}$). An error exists on the MEMS sensitivity accuracy, an order of magnitude below that of the geophone. Its influence on the sensor fidelity is all the more negligible as the sensitivity is not a frequency-dependent parameter, unlike damping and natural frequency. Unlike the case with MEMS sensors, which enable access to an accurate ground particle acceleration (or velocity after time integration), the designature process for geophones is approximate. As a matter of fact, this approximation is particularly large in the low frequencies.

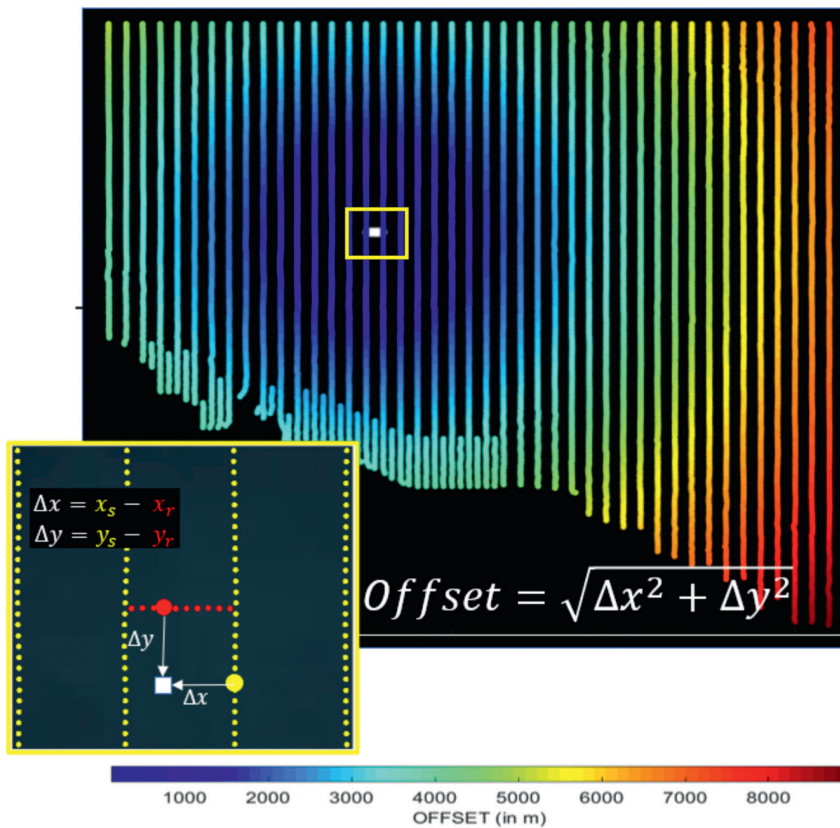


Figure 8 Elaboration of phase rings as a convenient QC tool for monitoring the spatial coherency of seismic signal. Sources are shown in yellow, OBN in red.

and requires considerable additional effort. Processing geophysicists would therefore use the nominal designature parameters provided in the manufacturer’s sensor specifications, without taking into account the tolerances. The designature process is then approximate (Figure 7, left). If surface-consistent processing jobs are used to smooth this approximation, the fact that the authors of this article found that the specifications of most geophones on the market did not follow a Gaussian distribution centred on their nominal value, means that the efficiency of this standard approach is less than ideal. (Tellier 2021).

The low frequencies acquired on the Abu Dhabi project were assessed for both the MEMS and hydrophone sensors. To do this, phase rings were used as a convenient way to validate the

spatial coherence of seismic signal phase as a SNR indicator. To produce these displays and duly visualise the low-frequency content (Figure 8), the seismic data were collected as an extended receiver gather over ten nodes. A Fast Fourier Transform was then computed for each trace and the phase component extracted. Phase components were then ordered in the X offset/Y offset plane and displayed at specific frequencies. Comparative sensor results are displayed in figure 9. Phase ring coherency down to 2 Hz on the Z MEMS indicates the clear dominance of signal over noise.

The ‘crispy’ aspect of hydrophone phase rings (Figure 9, left) at the lower frequencies is due to the presence of passive swell on top of the active seismic. The organisation of this

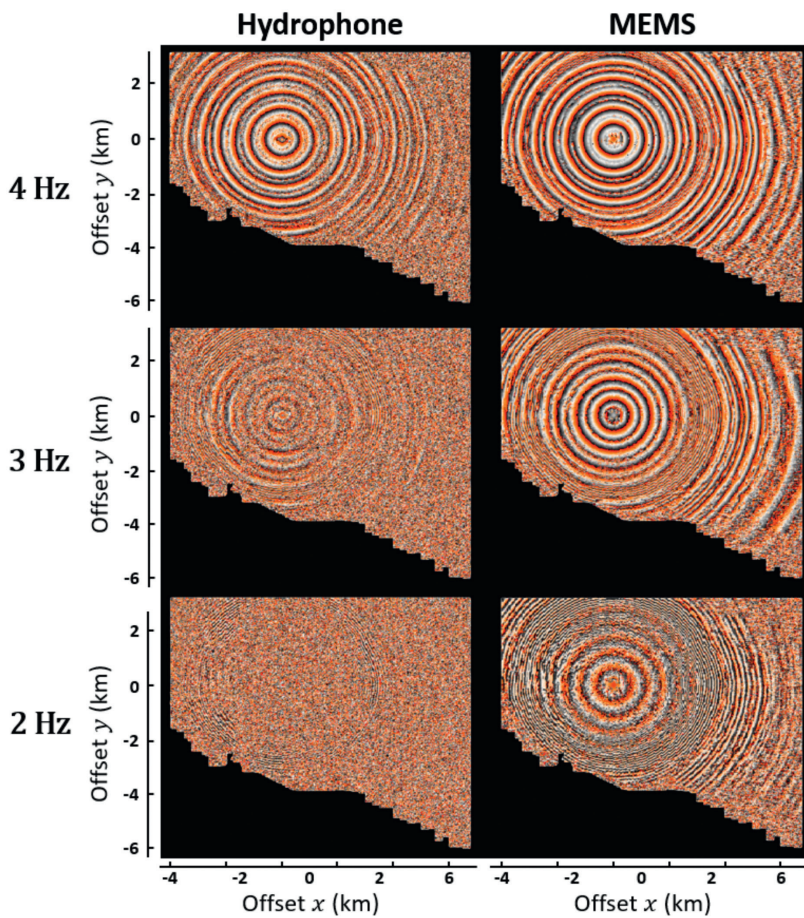


Figure 9 Phase rings of a GPR300 OBN equipped with a hydrophone (left) and 3C MEMS (right, Z component displayed only).

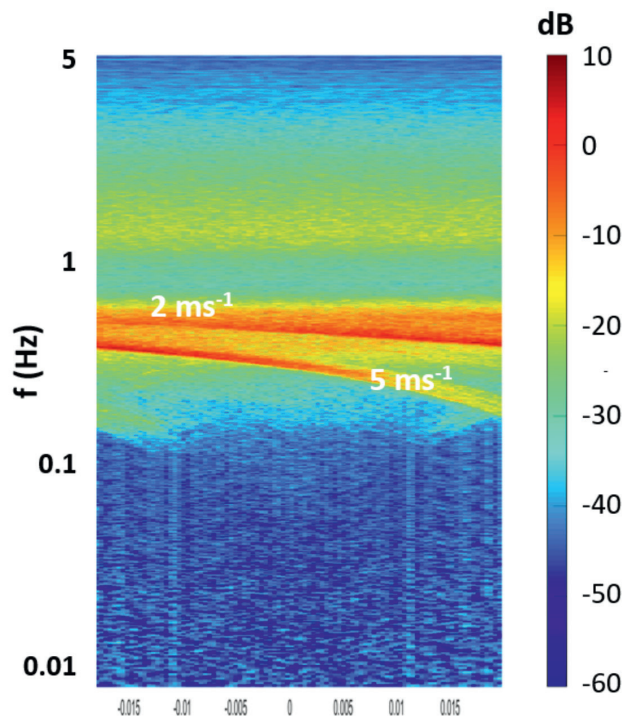


Figure 10 FK spectra of 50 GPR300 hydrophones with frequency logarithmic scale over a one-hour period of passive seismic recording.

swell noise is well illustrated on the FK amplitude spectrum (Figure 10) displaying 50 nodes over a period of passive recording time.

Outcome #6: continuous orientation monitoring

Reorientation of a node's three components into the project reference is one of the first steps performed when processing multi-component seismic data. The rotation angles (pitch/roll/heading) are usually estimated from a selected offset range of refracted data. The computed rotation angles may therefore differ from one estimation to the other, depending on the data range selected for this computation. Continuous measurement of the rotation angles at node level, enabled by the high-fidelity tilt measurement continuously performed by the 3C MEMS associated with the continuous compass measurement, offers an alternative solution for performing this reorientation.

Figure 11 illustrates this inherent capability. The node encountered a change in layout starting from shot No.12. The change in node layout is visible on the three node component (Figure 11, top), and is also recorded in the SEG-D metadata. The reorientation into the project reference can therefore be performed automatically (Figure 11 bottom). The phase continuity is in this way certified throughout the acquisition regardless of the project geometry and shooting sequence.

Outcome #7: accurate clock correction

Another OBN feature was studied during this commercial acquisition. Though not directly related to the sensing technology being used, timing accuracy is paramount when acquiring OBN surveys. The CSAC (Chip-scale atomic clock) is valued for its accuracy for long deployments in deep waters, but it is very costly, and there is controversy about its actual performance and

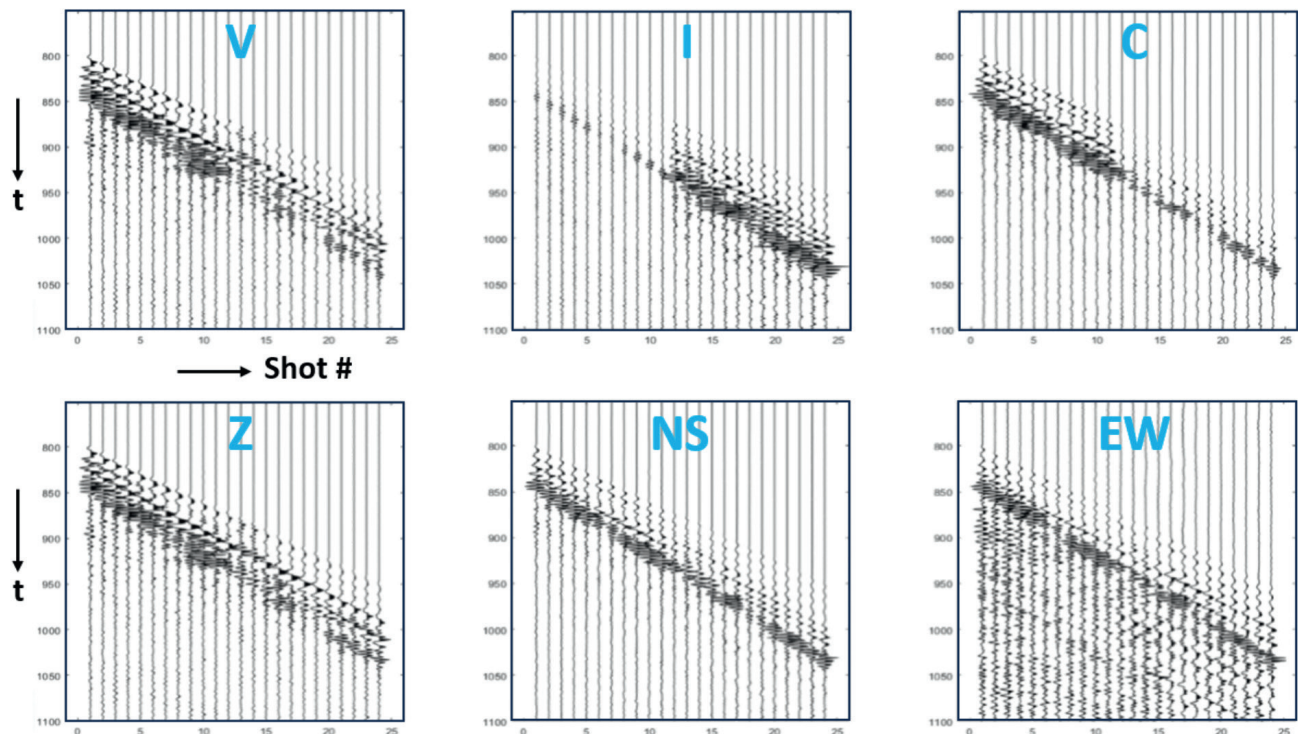


Figure 11 (Top) Shot gathers in the node referential (Vertical, Inline, Crossline) recorded at the time of a node move. (Bottom) Shot gathers delivered in the geographic referential after automated reorientation by the acquisition system.

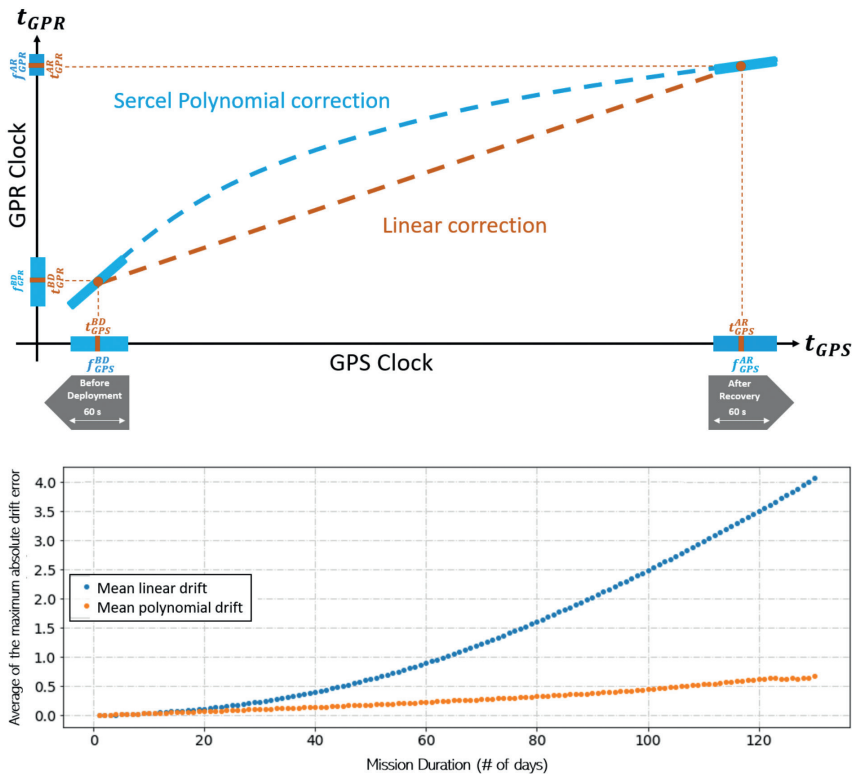


Figure 12 (Top) OBN clock drift correction. Single measurements at deployment and recovery enables application of a linear correction (orange). Enlarging the measurements (blue areas on the axes) enables the design of a polynomial correction. (Bottom) Statistical drift error according to mission duration.

real differentiation versus OCXO (Oven controlled crystal oscillator) clocks. For shallow applications with shorter deployments, OCXO can guarantee the typical mean timing error requirement of 1 ms @ 60 days after linear correction, and therefore remains the preferred industry option. In practice, a submerged OBN cannot receive the GPS signal. The nodes are synchronised with GPS prior to deployment. At recovery, the OBN clock time is

compared to the GPS time. The timing error at recovery can then be corrected. Values between deployment and recovery can be corrected too, with the common industry practice being the application of a linear correction (Figure 12 top, orange).

An alternative approach exists, however. Instead of single timing measurements at deployment and recovery, the nodes can be monitored for a short period of time, before deployment

straight after their synchronisation with GPS, and then again when retrieved. This short monitoring period allows access to the tendency of the time drift and thus enables the design of advanced, non-linear timing corrections (Figure 12 top, blue).

To validate this approach, 30 nodes were monitored in laboratory conditions, for two months and at a constant temperature, with no access to GPS but direct access to the node timing performed by its OCXO clock. GPS and OCXO timing was then available throughout the two-month experiment. Analysis of the data made it possible to design a fit-for-purpose polynomial timing correction (L'Her, 2018), constrained by the time and frequency difference of the OCXO and GPS clocks before deployment and after recovery. The polynomial correction significantly outperforms that of the linear correction (Figure 12, bottom). The error drift appears negligible when deployed for up to 25 days. It starts steadily diverging for longer deployments but still remains below 1 ms after slightly more than two months. At this point, the timing error proves to be three times less with the polynomial correction than with the linear correction. In operational terms this measurement process is short (< 1 min.) at both deployment and recovery.

This approach only proves to be efficient, however, if temperature variations are taken into account. Indeed, during operations, OBNs usually encounter different temperatures to those onboard the vessel, where the time drift and frequency drift measurements are made. While the oven compensation of OCXO addresses most of the temperature-related time drift, a residual time drift remains observable when temperature variations are present. To address this issue, regular temperature measurements are made in the vicinity of the OCXO, and an ad hoc solution applied. This feature has been implemented since the advent of the MEMS-based node and is in force on the two datasets presented above. It is interesting to note that an evolutionary convergence is observed on OCXO drift investigations and conclusions, although solutions differ (Bunting, 2023).

Conclusions

On the seabed, the sensing performance of 3C MEMS brings significant value to recorded datasets, as demonstrated on both an experimental acquisition and on the largest OBN commercial survey ever performed. In addition to their excellent sensing capability and fidelity at low frequencies, signal can be reconstructed with a true verticality, while the vector fidelity of the 3C axis is significantly improved. Direct benefits, such as advanced denoising and notch in-fill, are observable. For FWI purposes, unmatched low frequencies are expected to be obtained using a combination of MEMS-based OBNs with recently released marine low-frequency sources (Ronen 2017), especially given the demonstrated imaging capability of this source (Shang 2023). With MEMS sensors now equipping a full range of OBNs down to 6000 m, further positive results are to be expected from deep waters. MEMS sensors should therefore be a key driver in the expansion of OBN acquisition – especially for sparse, blended, velocity or 4D acquisitions, where sensing fidelity matters more than ever.

Acknowledgements

The authors would like to thank BGP Offshore and ADNOC as early adopters of MEMS-based OBN technology and for their support in analysing and further understanding the benefits of MEMS sensors. We would also like to thank the numerous Sercel colleagues who contributed to the success of the third MEMS generation and GPR300 design, test, industrialisation and industry delivery. Special acknowledgement goes to Didier Marin and Stéphane Laroche for their involvement and expertise in dataset analysis.

References

- Archer, J., Bell, L., Hall, M., Margrave, G., Hall, K. and Bertram, M. [2012]. Obtaining low frequency seismic data, onshore and in shallow water: *First Break*, **30**(1), 79-87. DOI: <https://doi.org/0.3997/1365-2397.30.1.56179>.
- Bunting, T. and Jurok, J. [2023]. Crystal Oscillators and Temperature Compensated Deterministic Clock Correction: third annual International Meeting for Applied Geoscience and Energy (IMAGE), extended abstract.
- Cambois, G., Al Mesaabi, S., Casson, G., Cowell, J. Mahgoub, M. and AL Kobaisi, A. [2019]. The world's largest continuous 3D onshore and offshore seismic survey sets ambitious quality and turnaround targets: SEG 89th Annual Meeting, expanded abstract. DOI: <https://doi.org/10.1190/segam2019-3214663.1>.
- Cordery, S. [2020]. An effective data processing workflow for broadband single-sensor single-source land seismic data: *The Leading Edge*, June 2020, 401-410. DOI: <https://doi.org/10.1190/tle39060401.1>.
- Keggin, J., Alaraji, W. and Zhou, J. [2017]. Improved images of fractured basement in Vietnam: *GeoExpro*, **14**(4), 22-25.
- Lainé, J. and Mougenot, D. [2014]. A high-sensitivity MEMS-based accelerometer: *The Leading Edge*, **33**(11), 1234-1242. DOI: <https://doi.org/10.1190/tle33111234.1>.
- L'Her, C. [2018]. Method and system for estimating the drift of a clock for dating seismic data samples, PCT patent application WO2020/002798.
- Ronen, S. and Chelminsky, S. [2017]. Tuned Pulse Source—a new low frequency seismic source. SEG 87th Annual Meeting, expanded abstract. DOI: <https://doi.org/10.1190/segam2017-w16-04.1>.
- Shang, X., Kryvohuz, M., Baeten, G., Macintyre, H., Perkins, C., Tang, Z., Theriot, C., Wang, K., Allemand, T., Aznar, J., Herrmann, P., Large, J., Laroche, S. and Ronen, S. [2023]. Imaging with a low frequency source: 84th EAGE annual conference and exhibition, expanded abstract. DOI: <https://doi.org/10.3997/2214-4609.202310617>.
- Tellier N. and Lainé, J. [2017]. Understanding MEMS-based digital seismic sensors. *First Break*, **35**(1), 93-100. <https://doi.org/10.3997/1365-2397.35.1.87386>.
- Tellier, N., Laroche, S., Wang, H. and Herrmann, Ph. [2021]. Single-sensor acquisition without data jitter: a comparative sensor study: *First Break*, **39**, 91-99. DOI: <https://doi.org/10.3997/1365-2397.fb2021007>.